This is an open access article published under a Creative Commons Attribution (CC-BY) License, which permits unrestricted use, distribution and reproduction in any medium, provided the author and source are cited.

ACS AuthorChoice

NANO LETTERS

Letter

pubs.acs.org/NanoLett

On-Chip Picosecond Pulse Detection and Generation Using Graphene Photoconductive Switches

Nicholas Hunter, Alexander S. Mayorov,* Christopher D. Wood, Christopher Russell, Lianhe Li, Edmund H. Linfield, A. Giles Davies, and John E. Cunningham

School of Electronic and Electrical Engineering, University of Leeds, Woodhouse Lane, Leeds LS2 9JT, United Kingdom

Supporting Information

ABSTRACT: We report on the use of graphene for room temperature on-chip detection and generation of pulsed terahertz (THz) frequency radiation, exploiting the fast carrier dynamics of light-generated hot carriers, and compare our results with conventional low-temperature-grown gallium arsenide (LT-GaAs) photoconductive (PC) switches. Coupling of picosecond-duration pulses from a biased graphene PC switch into Goubau line waveguides is also demonstrated. A Drude transport model based on the transient photoconductance of graphene is used to describe the mechanism for both detection and generation of THz radiation.

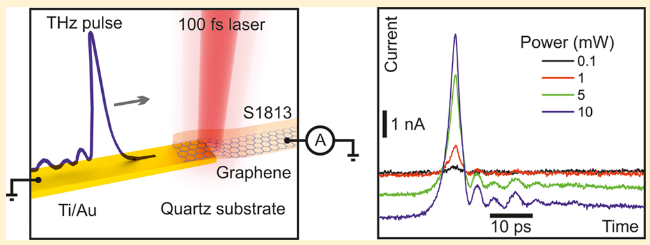

KEYWORDS: *Graphene, on-chip, THz detection, GaAs, Goubau line, photoconductive switch*

Since its discovery,[1] graphene has been shown to exhibit high room temperature carrier mobility,[2,3] a wide-band optical transparency in the infrared and visible light ranges,[4] and a short hot-carrier lifetime.[5] On the basis of these properties, graphene photodetection in the visible[6,7] and infrared[8] ranges of the electromagnetic spectrum has already been demonstrated. Furthermore, imaging of terahertz (THz) continuous wave fields by an antenna coupled to a metal gate of a graphene transistor[9] has recently been demonstrated, and the interaction between THz pulses and graphene in a free-space geometry has been studied.[10] On-chip (guided-wave) THz spectroscopy systems have several advantages in comparison with free-space techniques. For example, the confinement of the THz electric field close to a metal transmission line enhances the spatial resolution beyond the diffraction limit, and a high frequency−domain resolution (<1 GHz) is possible, since the geometry can allow a large etalon-free time−domain window. Graphene photodetection in on-chip systems has been demonstrated in the tens of GHz frequency range,[11,12] but to date not at higher frequencies (hundreds of GHz). Only pulsed THz generation has been demonstrated in graphene,[13] and then only with a pulse amplitude no larger than 10 pA for 0.2 mW incident optical beam power. Such studies do, however, imply that the fast carrier dynamics of photoexcited carriers (electron−hole pairs) in graphene could make it a powerful tool in the development of chip integrated THz communications devices.

The creation of photocarriers in graphene by the absorption of visible light (∼1.5 eV) has been studied extensively.[5] After ultrafast (∼10 fs) equilibration by carrier−carrier collisions, the resulting carrier distribution can be described by a Fermi−Dirac function with a time-dependent hot carrier temperature. A slower process, which affects the carrier distribution function, is optical phonon scattering, which occurs over a time scale of <0.1 ps. During this period, all hot electrons lose their energy, provided the energy is larger than the Debye energy (∼200 meV in graphene).[14] A process with an even longer time scale is electron/acoustic phonon scattering caused by thermalization between hot charge carriers and the lattice, which takes several nanoseconds.[15] Since this process is inefficient, supercollisions involving scattering with impurities are observed instead.[16,17] None of these scattering processes, however, change the total concentration of the photo-generated carriers; this is unlike the e−h recombination, which reduces the concentration over a short time (∼1 ps) and causes photoluminescence.[8] The e−h recombination depends sensitively on the properties of graphene (carrier concentration and temperature), as shown, for example, for the case of Auger recombination.[18]

Graphene is not traditionally used for THz photoconductive (PC) switches. Instead, low-temperature-grown gallium arsenide (LT-GaAs) PC-switches are typically used for the generation and/or detection of picosecond pulsed radiation in THz time−domain spectroscopy (THz-TDS) systems.[19,20] LT-GaAs is an ideal photoconductive switch material since it has a high mobility, high intrinsic resistivity, and the photogenerated carriers exhibit a short lifetime (of order 100 fs),[19,20] although careful temperature control is required during both the molecular beam epitaxial growth and subsequent annealing of the material. Generation and detection of THz pulses in both free-space and integrated on-chip systems are achieved by illumination of the photoconductive material by a subpicosecond duration laser pulse.[21,22] In on-chip THz-TDS

Received: October 27, 2014
Revised: February 5, 2015
Published: February 24, 2015

 © 2015 American Chemical Society

DOI: 10.1021/nl504116w
Nano Lett. 2015, 15, 1591−1596

systems, the THz field is then confined near a lithographically-defined metal transmission line, and interaction between the THz pulses and crystalline materials placed close to the transmission line can result in absorption at resonant frequencies, which can be detected by a second PC switch at the far end of the transmission line.[21,23]

In this paper we report on the generation of picosecond pulses using a LT-GaAs PC-switch and their detection using a graphene switch, where both switches are integrated into an on-chip Goubau-line waveguide. We compare the results with detection performed using standard LT-GaAs switches. Furthermore, we also demonstrate generation of a picosecond pulse in an on-chip system by using a biased graphene switch, comparing our results with previous work[13] in which generation of a picosecond pulse by unbiased graphene was demonstrated.

Two planar Goubau line devices, D1 and D2, were initially fabricated as shown in Figure 1. Both devices incorporated LT-GaAs PC switches (used for measurements and marked as LTA, LTO, and LTB) at either end of Goubau lines, but device D2 included graphene in a cross-geometry at the device center, extending across a 50 μm gap in the center conductor. Device fabrication proceeded as follows, with further details presented in the Supporting Information. First, epitaxial transfer was used to remove the LT-GaAs layer from its growth substrate and locate it on the quartz substrate. Device D1 comprised of a continuous 9-μm-wide and 2-mm-long center−conductor, separating two LT-GaAs PC switches (LTA and LTB). A graphene layer was transferred from its Cu growth substrate and subsequently etched into a cross-shape to form a four-terminal device, which we used to measure photocurrent and THz pulses in Device D2. The length of the transmission line between the LT-GaAs PC switch and the nearest graphene contact in device D2 was 1.07 mm. The graphene layer was coated by a 1.3-μm-thick layer of (Shipley 1813) photoresist during measurements in order to support the graphene structurally at the edges of the contacts, but it also served to protect it from ambient water absorption and to keep the doping level stable over time.

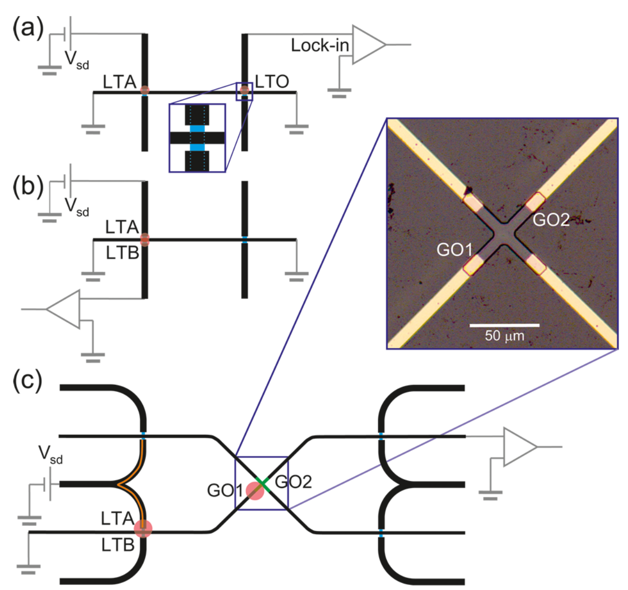

Figure 1. Schematic diagram of devices D1 and D2. (a) The setup for LT-GaAs "output" pulse detection in device D1. Gold electrodes are shown by black lines. For output pulse measurements a DC bias, V_{sd}, is applied to the PC switch LTA and a lock-in is connected to the PC switch LTO. The Goubau line is grounded throughout. The pump and probe beams, indicated by red circles, are focused on switches LTA and LTO, respectively. Inset: A part of a PC switch area where the blue color indicates LT-GaAs areas after etching. The dotted line indicates the edges of LT-GaAs under the metal contacts. (b) For "input" pulse measurements the probe beam and the lock-in are moved to the switch LTB, demonstrated for device D1. (c) Measurement setup for graphene detection in the device D2. Graphene is shown by a green cross, and the probe laser beam spot is focused on the spot GO1. The orange line indicates the path for the Fabry−Pérot reflections of THz pulse. Inset: Optical image of the quartz substrate with the graphene area etched in the shape of a cross covered by S1813 resist. The graphene has a length of 50 μm and width of 9 μm.

Since the observed response of the graphene PC switch (excluding a current offset, discussed later), is similar to that of a LT-GaAs PC switch, we were careful to rule out any residual LT-GaAs under the graphene layer from being a potential source of picosecond-pulse detection. No residues were detected by an optical microscope under a 150× lens magnification, and the Raman spectrum in the region of the graphene switch showed no evidence of photoluminescence from residual LT-GaAs (see Figure 2a). The Raman signal shows that our samples are composed from a single layer of graphene, as determined by the parameters extracted from a Lorentzian fit (peak positions, full width at half-maximum (FMHW), and the ratio of intensities) of the 2D- and G-peaks to the Raman spectrum obtained after removal of the background signal from quartz (Figure 2b).[24]

Pump−probe experiments were carried out using a pulsed Ti:sapphire laser centered at 790 nm, with a 100 fs pulse duration, and a repetition rate of 80 MHz. This beam was split into two, with the first branch used to illuminate a biased LT-GaAs PC switch for THz pulse generation and the second branch (the probe beam), focused onto a probe PC switch after being time-delayed using a retro-reflector on a delay stage, and chopped at 2827 Hz. The average power of both beams was 10 mW, and each beam spot had a FWHM of ∼35 μm (measured by scanning a knife edge in front of a calibrated power meter). For device D1, the resulting "output" THz pulse (see Figure 2c) transmitted down the Goubau line was detected at the LT-GaAs using a lock-in amplifier connected to one of the probe arms, as shown in Figure 1a. Reference measurements of the "input" THz pulse to the waveguide were also obtained by focusing the probe pulse on a region of LT-GaAs directly adjacent to the excitation point (generation at PC switch LTA and detection at switch LTB in Figure 1b). Similar "input" pulse measurements were performed for device D2 using switches LTA and LTB (Figure 1c) for comparison. It should be noted that four transmission lines could be used for the output pulse measurements in D2, but here the best performing LT-GaAs PC switches were chosen. Comparable input pulse shapes were generated in both devices D1 and D2 with FWHM equal to 1.65 ± 0.05 ps (the black curve in Figure 2c).

By comparing measurements of the input and output pulses in D1 (Figure 2c), it can be seen that dispersion of the propagating pulses occurs as they move down the transmission line causing a broadening of the output pulse (red curve) relative to the input pulse (black curve). The 12.2 ps delay between the pulses corresponds to a pulse velocity of 1.65 × 10^8 ms^{-1}. In comparison with the pulse detected by LT-GaAs in D1, the pulse detected by the graphene switch in D2 has a

DOI: 10.1021/nl504116w
Nano Lett. 2015, 15, 1591−1596

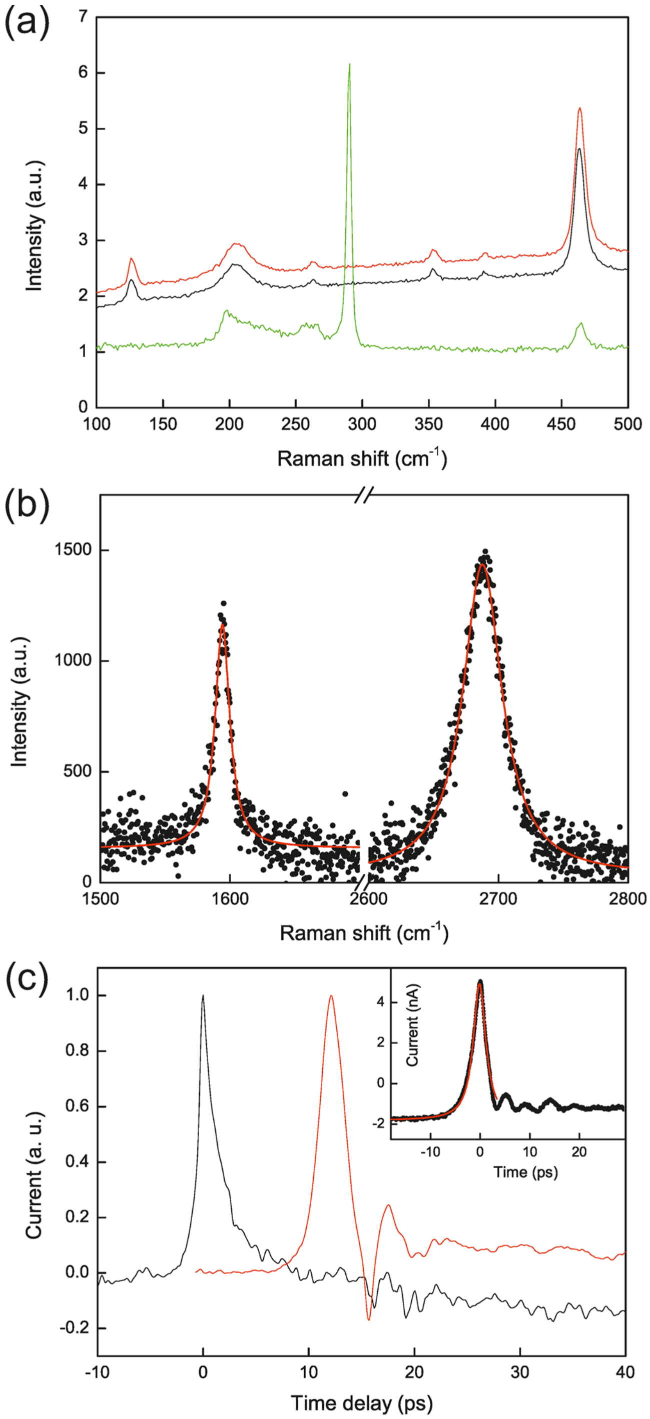

Figure 2. Characterization of graphene and LT-GaAs. (a) Raman spectra measured after excitation with a 633 nm laser for a clean quartz substrate (black), for the substrate after removal by etching of the LT-GaAs (red), and from an LT-GaAs covered region (green). No peak corresponding to LT-GaAs at 290 cm^{-1} was found in the graphene region. (b) Raman spectrum of a graphene switch region (black dots) and a Lorentzian fit of the G- and 2D-peaks (red). (c) Input pulse (normalized by 2.6 nA) generated at LTA and detected at LTB (black line), together with the output pulse (normalized by 0.35 nA) detected 2 mm away at LTO (red line) measured in the device D1 with LT-GaAs PC switches. The delay between the two pulses corresponds to a pulse propagation velocity in the Goubau line of 1.65 ± 0.02 × 10^8 ms^{-1}. Inset: Pulse detected by graphene at GO1 in device D2. The red line is a Lorentzian fit to the data.

similar peak shape but a negative background current offset (Figure 2c inset), the origin of which is discussed later.

A detailed comparison between the input pulse in D1 (black curve) and the pulse detected by the graphene in D2 (the red curve is plotted with the −1.7 nA DC offset removed) is given in Figure 3a. The measured delay of 6.3 ps between the input pulse and the detected pulse corresponds to the time taken for the pulse to travel the 1.07 mm of transmission line between PC switch LTA and the graphene−metal interface, GO1, due to the velocity in D2 being the same as device D1. It should be noted, though, that the input pulse measured in the device D2 (the black curve in Figure 3a) has several features not observed in the input pulse of the D1 Goubau line result shown in Figure 2c, namely a reflected pulse from the nearest ohmic contact due to impedance mismatch (at 12.5 ps, shown by the black arrow) and some small periodic oscillations detected after the main pulse (which are a factor of ∼10 smaller in amplitude). The frequency of these oscillations f_{osc} ∼220 GHz corresponds to a time delay $1/f_{osc}$ of ∼4.5 ps, and they are related to Fabry−Pérot reflections from geometric features in the probe arms, highlighted by the orange line in Figure 1c. The THz pulse can be reflected from the probe arms as well, but this was not observed in our measurement, since its amplitude is smaller than the amplitude of 220 GHz oscillations.

The inset to Figure 3a shows that the FWHM of the output pulse detected by LT-GaAs is 0.5 ps smaller than that of the pulse detected by graphene (FWHM is ∼3 ps) indicating slightly slower dynamics of the charge carriers in graphene compared with the LT-GaAs. Spectra obtained by fast Fourier transform (FFT) of the input pulse (D2), the output pulse detected by graphene (D2), and the output pulse detected by LT-GaAs (D1), shown in Figure 3b, allow us to define the frequency at which the signal is equal to the noise (∼0.6 THz for detection by both LT-GaAs and graphene). Since the shape and the noise level of the pulses detected by both the LT-GaAs and graphene PC switches are similar, we conclude that graphene PC switches can be used as picosecond pulses detectors for on-chip systems. Despite the small difference in geometry (namely, the detection by LT-GaAs in device D1 is performed using side contacts and for the detection by graphene, device D2, is in line with the transmission line), the shape of the detected pulse is similar in both devices since the PC switch can be viewed as a point-like detector when the wavelength (>100 μm) is much larger than a characteristic size of the detector ∼20 μm.

The detected current in a PC switch, $I(t)$, is a convolution of the transient THz electric field, E_{THz}, at the illuminated region, and the carrier dynamics described by a conductivity change, $\delta\sigma$:

$$I(t) \propto \int_{-\infty}^{+\infty} E_{THz}(\tau)\delta\sigma(t-\tau)\,d\tau \tag{1}$$

In the case of "ideal" detection with a very short rise/fall time, the conductivity change can be approximated as being proportional to a Delta function, and the detected current is proportional the electric field $I(t) \propto E_{THz}(t)$. In the case of LT-GaAs detection the conductivity change is defined by a life-time of the photoexcited carriers and dispersion as occurs in the output pulse measurement in device D1. However, our measurements are not sensitive enough to provide the time dependence of the graphene conductivity, owing to pulse dispersion in the Goubau line. To calculate the approximate conductivity change in our graphene switches, we deconvolute

DOI: 10.1021/nl504116w
Nano Lett. 2015, 15, 1591−1596

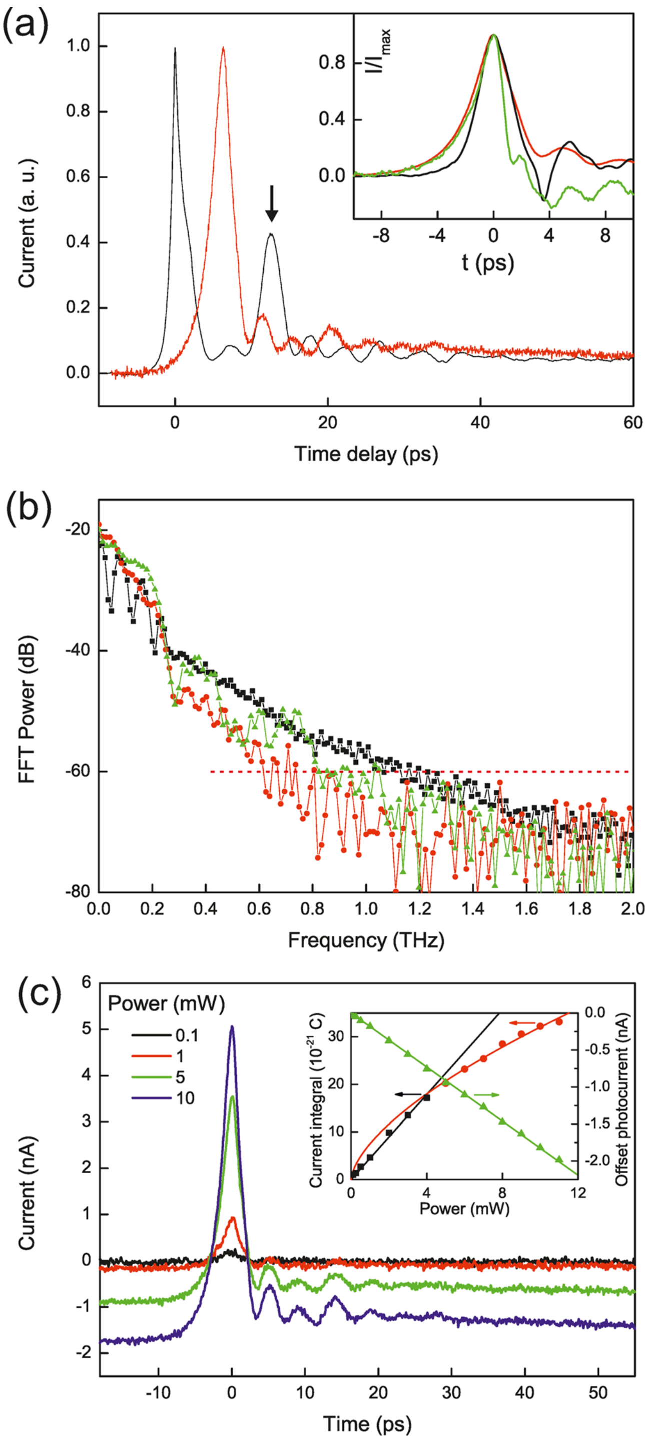

Figure 3. Characterization of THz pulse detection using graphene on device D2. (a) Input pulse (normalized by 75 nA) generated at LTA and detected at LTB (black line), and the output pulse (normalized by 6.7 nA) detected at GO1 by graphene (red line) measured in the device D2 repeated from Figure 2c inset, but with the current offset removed for comparison. A reflection from the graphene−metal interface is indicated by the black arrow. Inset: Normalized output pulses detected by LT-GaAs (in device D1) and graphene (in device D2), shown by black and red lines, respectively. Normalized conductivity change obtained from the deconvolution of the two output pulses shown in green. (b) FFT spectrum for the input pulse (device D2), output pulse detected by graphene (device D2), and output pulse detected by LT-GaAs (device D1) shown by black squares, red circles, and green triangles, respectively. The dashed red line indicates the chosen level of noise for the graphene detected signal

Figure 3. continued

used to define the bandwidth. (c) Pulse detected by graphene as a function of incident optical power. The DC current offset at −10 ps becomes more negative with increasing illuminating laser power. Inset: Lorentzian current integral as a function of incident power is shown by black squares in the linear region and red circles in the sub-linear region. Solid lines are power law fits, $\propto P^{\gamma}$, where $\gamma = 1$ and 0.6 for black and red curves, respectively. DC offset photocurrent as a function of incident power is shown by green triangles, obtained from a Lorentzian fit of the peak as shown on the inset in Figure 2c.

the signals.[25] We determined the FWHM of the conductivity change to be 2.2 ps from the shape of the resulting conductivity change plotted in the inset of Figure 3a by the green solid line, which is in agreement with the hot carrier life-time in graphene ~1.5 ps at room temperature previously reported (photon energy is 1.25 eV).[16]

We now discuss characterization of the graphene PC detector as a function of the probe beam power and the pump switch bias, to investigate the origin of the picosecond time scale detection mechanism in graphene further. Figure 3c shows the amplitude of the signal detected by the graphene PC switch as a function of probe power. A constant offset current, which depends on the illumination power, is observed, which is not observed in LT-GaAs PC switches. We have used a Lorentzian fit to extract the amplitude, width, and offset for each curve. An example of the fit is shown in the inset of Figure 2c, with a slight deviation from a Lorentzian shape observed for times larger than 2 ps originating from Fabry−Pérot reflections from the probe arms. The width of the detected pulse is ~3 ps for the largest probe powers (10 mW) and ~10% smaller for the smallest powers (1 mW). The time integral of the Lorentzian current pulse, used to calculate total charge transfer per optical pulse, is plotted in Figure 3c inset, together with the corresponding DC current offset, as a function of probe laser power. The offset current decreases linearly as the probe pulse power increases and is observed in the time domain both before and after the pulse. The charge as a function of incident power has a power−law dependence with an exponent equal to ~0.6 above 4 mW and ~1 below 4 mW as shown by the solid red and black lines, respectively. Since the amplitude of the THz pulse generated by switch LTA is proportional to V_{sd}, we measured the pulse detected at GO1 as a function of V_{sd} to investigate the linearity of the graphene response. The signal detected by graphene, as shown in Figure 4a, with a −1.7 nA DC offset removed, has a clear linear dependence on V_{sd}, and it can therefore be used as a linear detector for THz radiation.

Before we discuss the physical mechanism responsible for the detection of THz pulse using graphene, it is important to understand the properties of the metal−graphene interface. When undoped graphene is placed on top of a gold electrode it forms a weak bond; numerical calculations based on density-functional theory predict that a small p-type doping (~2.6×10^{12} cm^{-2}) arises with a Fermi energy shift equal to −0.19 eV for undoped graphene at zero temperature.[26] From the Raman data shown in Figure 2b we determined that our graphene-on-quartz has p-type doping of order $(6 \pm 2) \times 10^{12}$ cm^{-2}, using the widths, positions, and intensity ratio of the 2D and G Lorentzian peaks.[24] The metal−graphene junction will thus have a larger concentration of holes, p', on and near the metal, and a smaller concentration in the bulk, p. This $p'-p$ interface is responsible for the DC photocurrent in graphene. When no

DOI: 10.1021/nl504116w
Nano Lett. 2015, 15, 1591−1596

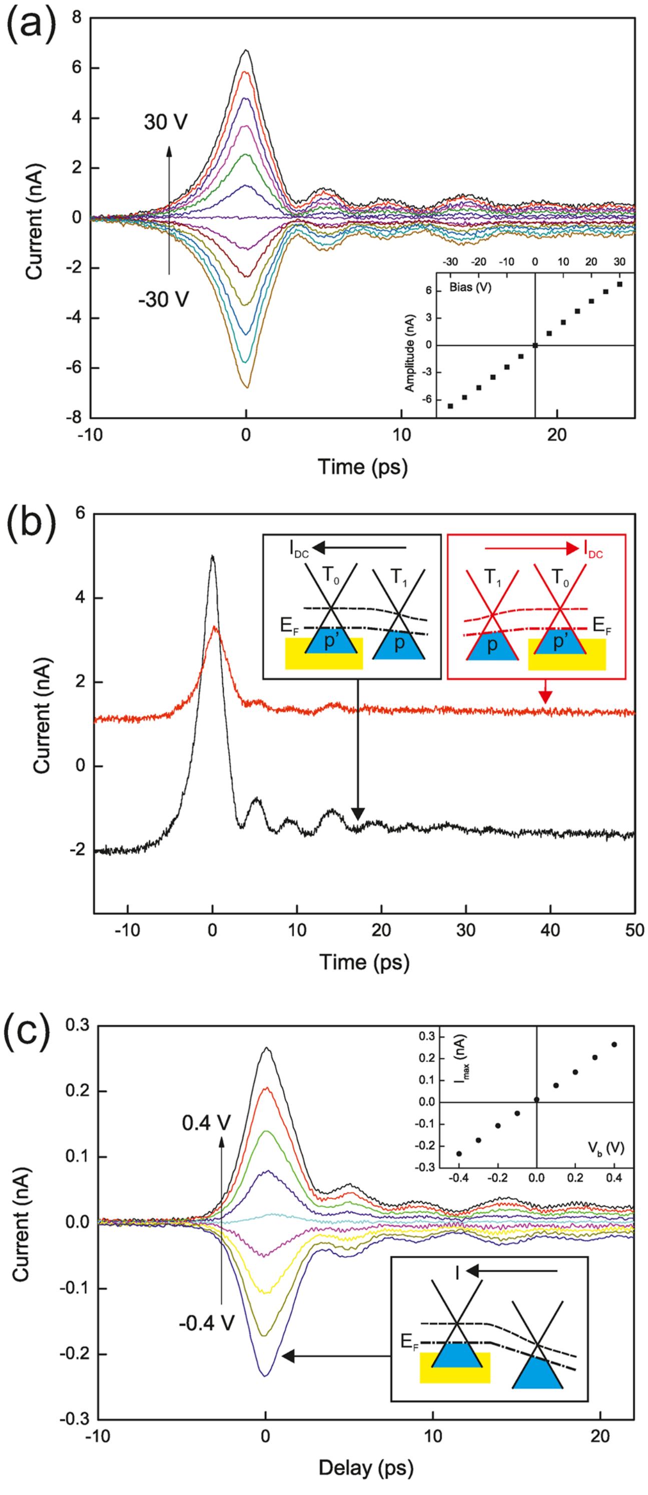

Figure 4. THz pulse detected by graphene and generation by biased graphene. (a) Pulse detected by graphene as a function of the source–drain bias applied to the LT-GaAs PC switch at 10 mW pump and probe powers. The applied bias changes with 5 V steps between the most negative signal, measured at −30 V, to the most positive signal, measured at 30 V. A DC current offset corresponding to −1.7 nA has been subtracted from the signal for clarity. Inset: Amplitude of the pulse as a function of the PC switch bias. (b) Pulse detection on the nearest and the furthest graphene ohmic contacts indicated by GO1 (black) and GO2 (red) in Figure 1c, respectively. The position of the THz pulse detected at GO1 is taken as a reference. Inset: Band structure of graphene without applied bias near an ohmic contact. As soon as the temperature, T_1, of the illuminated graphene is larger than

Figure 4. continued

the temperature of graphene placed on the metal contact (yellow area), T_0 = 300 K, and p' is larger than p, a DC photothermoelectric current flows toward the contact.[14] (c) The pulse generated by graphene on GO1 and detected by the LT-GaAs PC switch LTA as a function of a DC bias applied to the graphene using 10 mW pump and probe powers. The setup for THz pulse generation by graphene is shown in Supporting Information. Top inset: Current amplitude as a function of the applied bias. Bottom inset: Band structure for the graphene under applied negative bias. The bias generates a negative THz pulse if the conductivity change under illumination is positive.

bias is applied to the illuminated graphene, a DC current, I_{DC}, flows across this interface toward a cold gold contact owing to the photothermoelectric effect,[14] as shown on the inset in Figure 4b. A photothermoelectric origin for the DC offset was further confirmed by moving the probe beam focus from the metal–graphene interface at the nearest ohmic contact, GO1, to the furthest graphene–metal interface at GO2. The DC offset changed its sign as expected, as shown in Figure 4b. Another possible contribution to the DC offset, the photovoltaic effect, was found to be negligible in our experiment, since we did not observe any difference in the photocurrent as a function of laser beam polarization angle (see Supporting Information).[27] Since the polarity of the THz pulse did not change sign, the pulse detection cannot be attributed to either photoelectric or photo–thermoelectric effects. The amplitude of the detected pulse becomes smaller due to losses in graphene. A small delay of 0.4 ± 0.1 ps between the pulses is attributed to a time required for the THz field to travel from GO1 to GO2. This means that graphene detection may be used to measure the THz field spatially as it propagates across the graphene region.

The interaction of light with graphene is well-understood. Graphene absorbs only 2.3% of the total incident power from a sub–ps pulse from an 800 nm laser.[4] The internal quantum efficiency of graphene is, however, high, so almost all absorbed photons generate e–h pairs. For a short period of illumination, the probe pulse changes the electron (hole) concentration in graphene, which can be estimated for a single laser pulse as

$$\delta n(P) = \alpha \frac{P}{SrE_g} \tag{2}$$

where α is the part of the total light power absorbed by graphene (2.3%), P is the illuminating laser power (∼20 mW), E_g is the light quanta energy (1.6 eV), r is the number of pulses received per second, and S is the area of the spot. Thus, the change of concentration during a single pulse is expected to be less than 6×10^{11} cm^{-2}, which is 1 order of magnitude smaller than the graphene doping level, as determined by Raman spectroscopy.

Using a Drude model, the concentration change after illumination can affect the conductivity of graphene in two ways. In the linear regime, when the laser incident power is less than 4 mW, the mobility μ is unaffected by incident power. The conductivity change is directly proportional to concentration $\delta\sigma(P) \sim e\mu\delta n(P)$, where e is the elementary charge, and any applied bias will cause a current flow. In our experiment such a bias is provided by the THz electric field. A sublinear regime of detection is found above 4 mW power as shown in the inset to Figure 3c. This point indicates a regime when mobility change cannot be neglected. Though a change of mobility, $\delta\mu(P)$,

DOI: 10.1021/nl504116w
Nano Lett. 2015, 15, 1591−1596

accounts for a change of conductivity, $\delta\sigma(P)$, in the nonlinear function of power $\delta\sigma(P) \sim e\mu\delta n(P) + en_0\delta\mu(P)$, where n_0 is the concentration without illumination.

In further support of a photoconductive detection mechanism, we have also measured the inverse effect wherein a THz pulse is generated by a DC bias applied across graphene, which changes the graphene conductance by illumination, with detection then achieved by an LT-GaAs PC switch. The pulse amplitude is found to be proportional to the applied DC bias, and the current amplitude (Figure 4c inset) has a linear dependence on the applied bias. We notice that a pulse with a small amplitude of 13 pA can be measured even at zero applied bias. A similar current amplitude of ∼10 pA was previously observed in unbiased graphene, using a laser (1.6 eV) of 0.2 mW power and spot size of 2 μm, and attributed to a transient displacement current density and photothermoelectric effect.[13]

In conclusion, we have demonstrated THz pulse detection by graphene in an on-chip system. The graphene switch was found to have a linear response to both THz pulse amplitude and probe beam intensity. We identify the transient photoconductivity change due to light absorption as the mechanism for THz pulse detection. Our study paves the way for the creation of purely graphene-based on-chip THz sensors. In order to reduce dispersion in such devices, the transit path for the picoseond pulse could be shortened, or the substrate thinned by lapping to reduce the effective refractive index.[28]

■ ASSOCIATED CONTENT

Supporting Information

Device fabrication and THz pulse detection by graphene as a function of polarization. Two-terminal graphene device. This material is available free of charge via the Internet at http://pubs.acs.org.

■ AUTHOR INFORMATION

Corresponding Author

*E-mail: mayorov@gmail.com.

Notes

The authors declare no competing financial interest.

■ ACKNOWLEDGMENTS

We acknowledge funding from EPSRC, ERC grants NOTES and TOSCA, the National Physical Laboratory, and support from the Royal Society and the Wolfson Foundation. We are grateful to F. Guinea and J. Wu for fruitful discussions and Dr. Oscar Céspedes for use of the Raman spectrometer.

■ REFERENCES

(1) Novoselov, K. S.; Geim, A. K.; Morozov, S. V.; Jiang, D.; Zhang, Y.; Dubonos, S. V.; Grigorieva, I. V.; Firsov, A. A. *Science* **2004**, *306*, 666.

(2) Morozov, S. V.; Novoselov, K. S.; Katsnelson, M. I.; Schedin, F.; Elias, D. C.; Jaszczak, J. A.; Geim, A. K. *Phys. Rev. Lett.* **2008**, *100*, 016602.

(3) Dean, C. R.; Young, A. F.; Meric, I.; Lee, C.; Wang, L.; Sorgenfrei, S.; Watanabe, K.; Taniguchi, T.; Kim, P.; Shepard, K. L.; Hone, J. *Nat. Nanotechnol.* **2010**, *5*, 722.

(4) Nair, R. R.; Blake, P.; Grigorenko, A. N.; Novoselov, K. S.; Booth, T. J.; Stauber, T.; R. Peres, N. M.; Geim, A. K. *Science* **2008**, *320*, 1308.

(5) Bonaccorso, F.; Sun, Z.; Hasan, T.; Ferrari, A. C. *Nat. Photonics* **2010**, *4*, 611.

(6) Gabor, N. M.; Song, J. C. W.; Ma, Q.; Nair, N. L.; Taychatanapat, T.; Watanabe, K.; Taniguchi, T.; Levitov, L. S.; Jarillo-Herrero, P. *Science* **2011**, *334*, 648.

(7) Xia, F.; Mueller, T.; Lin, Y.; Valdes-Garcia, A.; Avouris, P. *Nat. Nanotechnol.* **2009**, *4*, 839.

(8) Liu, C.-H.; Chang, Y.-C.; Norris, T. B.; Zhong, Z. *Nat. Nanotechnol.* **2014**, *9*, 273.

(9) Vicarelli, L.; Vitiello, M. S.; Coquillat, D.; Lombardo, A.; Ferrari, A. C.; Knap, W.; Polini, M.; Pellegrini, V.; Tredicucci, A. *Nat. Mater.* **2012**, *11*, 865.

(10) Shi, S.-F.; Tang, T.-T.; Zeng, B.; Ju, L.; Zhou, Q.; Zettl, A.; Wang, F. *Nano Lett.* **2014**, *14*, 1578.

(11) Gan, X.; Shiue, R.-J.; Gao, Y.; Meric, I.; Heinz, T. F.; Shepard, K.; Hone, J.; Assefa, S.; Englund, D. *Nat. Photonics* **2013**, *7*, 883.

(12) Youngblood, N.; Anugrah, Y.; Ma, R.; Koester, S. J.; Li, M. *Nano Lett.* **2014**, *14*, 2741.

(13) Prechtel, L.; Song, L.; Schuh, D.; Ajayan, P.; Wegscheider, W.; Holleitner, A. W. *Nat. Commun.* **2012**, *3*, 646.

(14) Song, J. C. W.; Rudner, M. S.; Marcus, C. M.; Levitov, L. S. *Nano Lett.* **2011**, *11*, 4688.

(15) Bistritzer, R.; MacDonald, A. H. *Phys. Rev. Lett.* **2009**, *102*, 206410.

(16) Graham, M. W.; Shi, S.-F.; Wang, Z.; Ralph, D. C.; Park, J.; McEuen, P. L. *Nano Lett.* **2013**, *13*, 5497.

(17) Song, J. C. W.; Reizer, M. Y.; Levitov, L. S. *Phys. Rev. Lett.* **2012**, *109*, 106602.

(18) Rana, F. *Phys. Rev. B* **2007**, *76*, 155431.

(19) Gupta, S.; Frankel, M. Y.; Valdmanis, J. A.; Whitaker, J. F.; Mourou, G. A.; Smith, F. W.; Calawa, A. R. *Appl. Phys. Lett.* **1991**, *59*, 3276.

(20) Gregory, I. S.; Baker, C.; Tribe, W. R.; Evans, M. J.; Beere, H. E.; Linfield, E. H.; Davies, A. G.; Missous, M. *Appl. Phys. Lett.* **2003**, *83*, 4199.

(21) Auston, D. H.; Cheung, K. P.; Smith, P. R. *Appl. Phys. Lett.* **1984**, *45*, 284.

(22) Gacemi, D.; Mangeney, J.; Colombelli, R.; Degiron, A. *Sci. Rep.* **2012**, *3*, 1369.

(23) Byrne, M. B.; Cunningham, J.; Tych, K.; Burnett, A. D.; Stringer, M. R.; Wood, C. D.; Dazhang, L.; Lachab, M.; Linfield, E. H.; Davies, A. G. *Appl. Phys. Lett.* **2008**, *93*, 182904.

(24) Das, A.; Pisana, S.; Chakraborty, B.; Piscanec, S.; Saha, S. K.; Waghmare, U. V.; Novoselov, K. S.; Krishnamurthy, H. R.; Geim, A. K.; Ferrari, A. C.; Sood, A. K. *Nat. Nanotechnol.* **2008**, *3*, 210.

(25) Using a Matlab function deconv(f1,f2) with the pulse detected by graphene as f1 and the output pulse shown in Figure 2c as f2.

(26) Khomyakov, P. A.; Giovannetti, G.; Rusu, P. C.; Brocks, G.; van den Brink, J.; Kelly, P. J. *Phys. Rev. B* **2009**, *79*, 195425.

(27) Echtermeyer, T. J.; Nene, P. S.; Trushin, M.; Gorbachev, R. V.; Eiden, A. L.; Milana, S.; Sun, Z.; Schliemann, J.; Lidorikis, E.; Novoselov, K. S.; Ferrari, A. C. *Nano Lett.* **2014**, *14*, 3733.

(28) Russell, C.; Wood, C. D.; Burnett, A. D.; Li, L.; Linfield, E. H.; Davies, A. G.; Cunningham, J. E. *Lab Chip* **2013**, *13*, 4065.

DOI: 10.1021/nl504116w
Nano Lett. 2015, 15, 1591−1596